International Journal of Engineering

A Novel Volcano Smoke Antenna with Optimal Shape

K. Paran*[a], A. Abolghasemi [b]

[a] *Department of Electrical and Computer Engineering, S. Beheshti University, Tehran, Iran*
[b] *Department of Communications Technology, Research Institute for information and Communications Technology, Tehran, Iran*

A B S T R A C T

The design of a novel volcano smoke antenna for UWB indoor applications is presented. The design method is based on a general description for the geometry of UWB monopole antennas which is capable of producing most possible shapes for these antennas. It is also compatible with different optimization methods. In addition to a volcano smoke antenna, this method is used to design two optimized monopole antennas with flat and shaped grounds. The optimization of antennas is carried out by applying a hybrid procedure which begins with a GA global search and completes with a local search. The optimization process aims at minimizing the reflection coefficient of antennas over the operating band while reducing the time-domain distortion of radiated pulses. For Shaped ground and volcano smoke antennas, the reduction of variations in the energy pattern has been added to the optimization goals. The numerical results show the reliability and effectiveness of the whole process. These results also show considerable improvement regarding the size and operational characteristics of the antenna in comparison with similar antennas reported in the literature. The operational characteristics of shaped ground and volcano smoke antennas show that by shaping the ground, better performance could be achieved with smaller radiating elements and ground planes.

doi: 10.5829/idosi.ije.2013.26.03c.06

1. INTRODUCTION

The volcano smoke antenna has been proposed in 1945 by J. D. Kraus [1] as a wideband omnidirectional antenna. The key feature of this antenna is the particular shape of ground and radiating element which provides an uninterrupted and smooth transition of wave from feed line to free space (or vice versa). This results in low return loss in a wide frequency band as well as low time-domain distortion of the waveform. In spite of these suitable characteristics, practical applications of this antenna are very limited due to its voluminous configuration.

Since the allocation of the 3.1-10.6 GHz spectrum by the Federal Communications Commission (FCC) for ultra-wideband (UWB) radio applications [2], the interest in this technology has greatly increased. Attractive features like immunity to interferences and noise, extremely low emission levels, and high-speed data transmission make the UWB a promising technology. In UWB radio systems, unlike conventional narrowband systems, antennas are transmitting or receiving sub-nanosecond base-band pulses. Consequently, the traditional frequency-domain description and characterization of antennas behavior and performance are not adequate for UWB antennas. Therefore, the selection and design of antennas for UWB systems should be accomplished in a comprehensive manner taking into account not only the impedance matching over the operating band, but also the time-domain distortion of pulses and pattern characteristics [3-5]. The volcano smoke antenna seems to be a good choice for UWB systems. Several works have been done since 2002 to design an optimal volcano smoke antenna suitable for UWB applications [6-9].

Optimization of UWB antennas are mostly done by choosing a particular shape and tuning its geometrical parameters [9-12].

In some works, optimization has been performed not to obtain the optimum parameters of a particular shape, but to find the optimal shape of the antenna [13-18].

In these works, the geometry of antennas is described in a general manner allowing the antennas to take different shapes during the optimization process.

*Corresponding Author Email: *K_Paran@sbu.ac.ir* (K. Paran)

However, none of these general descriptions could produce all or most of the possible shapes for that type of antenna. Some of these general descriptions are also incompatible with some optimization methods like genetic algorithm (GA). For example, the crossover between two acceptable shapes may generate one or two unacceptable (e.g. self-intersecting) shapes.

In this paper, the design of a novel volcano smoke antenna for UWB applications is described. The design method is based on a general description for the geometry of UWB monopole antennas (proposed by authors in [19]) which is capable of producing most possible shapes for these antennas. Constraints could be set for dimensions of the antennas. This general description is also compatible with different optimization methods (especially GA). In this way, the optimal shape of volcano smoke antenna for a particular application could be found by an optimization process.

During the optimization process, the electromagnetic analysis of antennas is carried out by a finite-difference time-domain (FDTD) simulator, the RSS-FDTD code, which is an efficient tool for analyzing the rotationally-symmetric structures. The optimization of antennas is performed by applying a hybrid procedure which begins with a GA search and completes with a pattern search [20, 21]. The optimization procedure aims at minimizing the reflection coefficient of antennas over the operating band while reducing the time-domain distortion of radiated pulses. In some cases, the reduction of variations in the energy pattern is also considered as an optimization goal.

The paper is organized as follows: The key parts of the optimization setup, including the general description of antennas geometry, the electromagnetic simulator, the objective function, and the optimization procedure are discussed in the next section. Samples of numerical results are presented in section 3 to show the effectiveness of the proposed approach. Section 4 summarizes the paper.

2. OPTIMIZATION PROCESS

During the optimization process, the "optimization tool" generates set or sets of parameters at each iteration. Each set of parameters corresponds to an antenna according to the "general description of antennas geometry". Antennas are analyzed using an "electromagnetic simulator" and for each antenna, the value of objective function is calculated. This value shows the fitness of the antenna with regard to the optimization goals. At subsequent iterations, the optimization tool uses these values and the corresponding sets of parameters to generate new sets of parameters which are expected to exhibit better fitness. The key parts of the optimization setup are discussed in this section.

2. 1. General Description of Antenna Geometry
The shaped ground and shaped radiating element, which are the key features of the volcano smoke antenna, could provide an uninterrupted and smooth transition of radiating pulse from feed line to free space that results in low return loss over the frequency band and reduces the time domain distortion of radiating waveform.

The proposed scheme to generally describe the geometry of a rotationally-symmetric volcano smoke antenna with finite ground plane is illustrated in Figure 1. The primary profile of the antenna is formed by 12 control points, 4 points for shaping the ground (U_0-U_3), 4 points for shaping the lower part of radiating element (V_0-V_3), and 4 points for shaping the upper part of radiating element (W_0-W_3). The final profile consists of one rectangle (the cross-section of lower plate) and two splines (one forming the cross-section of shaped ground and the other forming the cross-section of radiating element). In Figure 1, a, b, c, and l are the geometrical parameters of the feeding coaxial line and t is the thickness of lower plate. Moreover, $\Delta\rho_{max}$ is the maximum allowable distance between the control points and the outer conductor of coaxial line, Δz_{max} is the maximum allowable distance between control points and ρ–axis, $\Delta\rho_{grd}$ is the maximum allowable range for ground plane to extend beyond the shaped part, $\Delta\rho_{mar}$ is the margin along the ρ–direction, and Δz_{mar} is the margin along the z–direction.

The first control point of the ground (U_0) is positioned along the outer conductor of coaxial line ($\rho = b$), the first control point of the lower part of radiating element (V_0) is positioned along the inner conductor of coaxial line ($\rho = a$), and the first control point of the upper part of radiating element (W_0) is positioned on the axis of symmetry ($\rho = 0$). Second points (U_1, V_1, W_1), third points (U_2, V_2, W_2), and forth points (U_3, V_3, W_3) are positioned at same distance from the axis of symmetry ($\rho = \rho_1$, $\rho = \rho_2$, and $\rho = \rho_3$ respectively). ρ_3 is between ρ_{31} and ρ_{max} where $c < \rho_{31} < \rho_{max}$, ρ_2 is between ρ_{21} and ρ_{22}, and ρ_1 is between ρ_{11} and ρ_{12} where $c < \rho_{11} < \rho_{12} < \rho_{21} < \rho_{22} < \rho_3$.

The last control point of the ground (U_3) is positioned on ρ–axis and other control points of the ground are below a specified level ($0 < z_{U_i} < z_{U_{12}}$, i = 0, 1, 2). U_0 is also below V_0 ($z_{U_0} < z_{V_0}$). V_0 is below

a specified level ($z_{V_0} < z_{V_{11}}$) and other control points of the lower part of radiating element are between $z = z_{V_{11}}$ and $z = z_{V_{12}}$ ($z_{V_{11}} < z_{V_i} < z_{V_{12}}$, i = 1, 2, 3). Each control point of the upper part of radiating element is between the corresponding control point of the lower part and $z = z_{max}$ ($z_{V_i} < z_{W_i} < z_{max}$, i = 0,1,2,3) .

The position of control points and the radius of ground plane could be determined by the following equations:

$$\rho_{31} = r_{31}\Delta\rho_{max} + c \quad , \quad 0 < r_{31} < 1 \tag{1}$$

$$\rho_3 = r_3(\rho_{max} - \rho_{31}) + \rho_{31} \quad , \quad 0 < r_3 < 1 \tag{2}$$

$$\rho_{ij} = r_{ij}(\rho_3 - c) + c \quad , \quad 0 < r_{ij} < 1 \quad , \quad i, j = 1, 2 \tag{3}$$

$$\rho_i = r_i(\rho_{i2} - \rho_{i1}) + \rho_{i1} \quad , \quad 0 < r_i < 1 \quad , \quad i = 1, 2 \tag{4}$$

$$\rho_{41} = (\rho_{max} + \rho_3)/2 \tag{5}$$

$$\rho_{42} = \rho_{41} + \Delta\rho_{grd} \tag{6}$$

$$\rho_4 = r_4(\rho_{42} - \rho_{41}) + \rho_{41} \quad , \quad 0 < r_4 < 1 \tag{7}$$

$$z_{U_{12}} = u_{12}\Delta z_{max} \quad , \quad 0 < u_{12} < 1 \tag{8}$$

$$z_{V_{1j}} = v_{1j}\Delta z_{max} \quad , \quad 0 < v_{1j} < 1 \quad , \quad j = 1, 2 \tag{9}$$

$$z_{U_0} = \min(u_0 z_{V_0}, z_{U_{12}})$$
$$= \min(u_0 v_0 z_{V_{11}}, z_{U_{12}}) \quad , \quad 0 < u_0, v_0 < 1 \tag{10}$$

$$z_{U_i} = u_i z_{U_{12}} \quad , \quad 0 < u_i < 1 \quad , \quad i = 1, 2 \tag{11}$$

$$z_{V_0} = v_0 z_{V_{11}} \quad , \quad 0 < v_0 < 1 \tag{12}$$

$$z_{V_1} = v_1(z_{V_{12}} - z_{V_{11}}) + z_{V_{11}} \quad , \quad 0 < v_1 < 1 \tag{13a}$$

$$z_{V_2} = v_2(z_{V_{12}} - z_{V_{11}}) + z_{V_1} \quad , \quad 0 < v_2 < 1 \tag{13b}$$

$$z_{V_3} = v_3(z_{V_{12}} - z_{V_{11}}) + z_{V_2} \quad , \quad 0 < v_3 < 1 \tag{13c}$$

$$z_{W_i} = w_i(z_{max} - z_{V_i}) + z_{V_i} \quad , \quad 0 < w_i < 1 \quad , \quad i = 0,1,2,3 \tag{14}$$

Equation (13) guarantees a positive slope at any point on the lower part of radiating element.
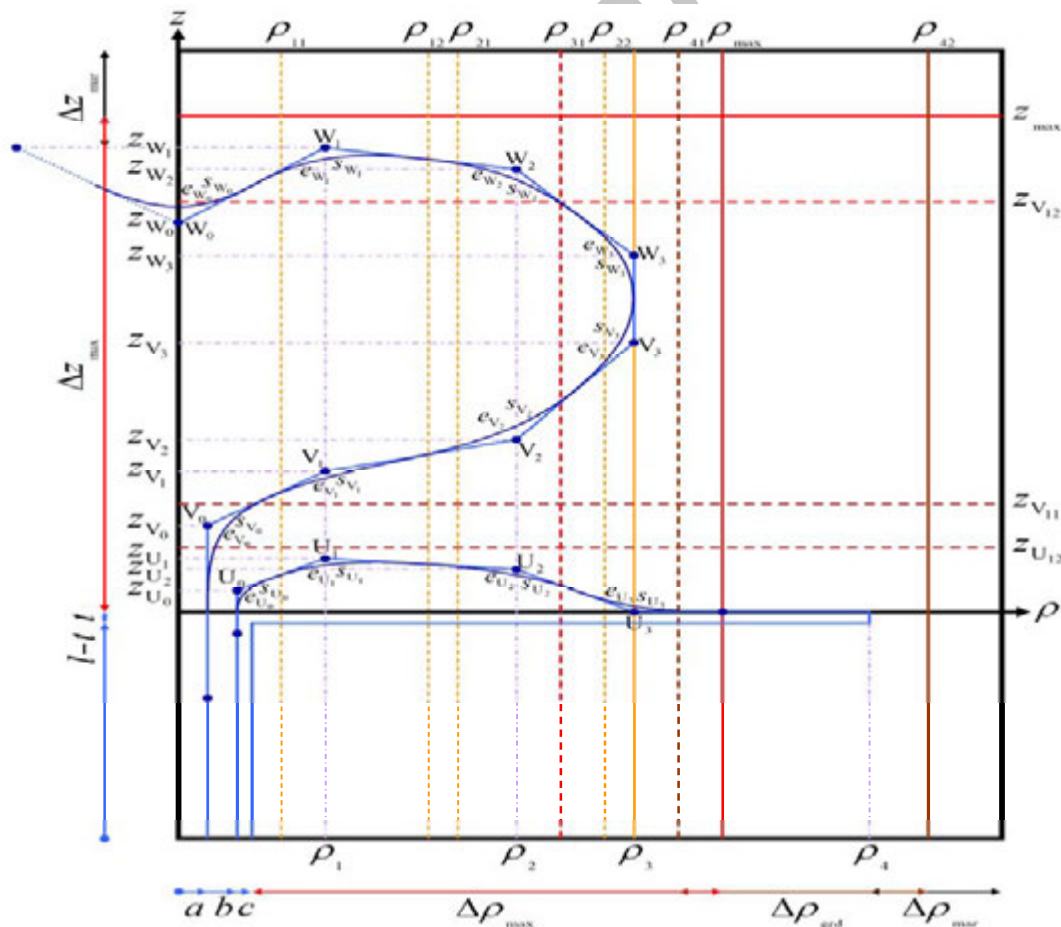

Figure 1. The proposed scheme to generally describe the geometry of a rotationally-symmetric volcano smoke antenna with finite ground plane.

Special kind of spline is used to derive the final profile. This spline replaces each edge of a given polygon by a curve with specified expansion and sharpness, which are determined respectively by expansion and sharpness factors assigned to that edge. Figures 2 and 3 show the replacement of an open polygon with splines, considering different expansion and sharpness factors, respectively. An expansion and a sharpness factor should be assigned to each control point shown in Figure 1 ($0 < e_{X_i}, s_{X_i} < 1$, $X \equiv U, V, W$, $i = 0, 1, 2, 3$). a, b, c, l, t, $\Delta\rho_{max}$, Δz_{max}, $\Delta\rho_{grd}$, $\Delta\rho_{mar}$, Δz_{mar}, r_{11}, r_{12}, r_{21}, r_{22}, r_{31}, u_{12}, v_{11}, and v_{12} are constant parameters which are appointed prior to the optimization process according to the dimensions of the feeding cable or connector and the desired sizes of radiating element and ground. r_1, r_2, r_3, r_4, u_0, u_1, u_2, v_0, v_1, v_2, v_3, w_0, w_1, w_2, w_3, e_{X_i}, and s_{X_i} ($X \equiv U, V, W$, $i = 0, 1, 2, 3$), each could be considered as a constant parameter or an optimization parameter.

A wide variety of shapes could be generated using the proposed scheme, including polygons with sharp edges, polygons with rounded edges and different curved shapes. The proposed scheme never generates self-intersecting or discontinuous shapes. An uninterrupted and smooth transition of radiating pulse from feed line to free-space could be readily provided by shaping the cross-section of radiating element (especially its lower part) and the cross-section of ground in a proper manner, which can be carried out by finding the best positions for control points and the optimum values of spline factors through an optimization process. This general description is compatible with different optimization methods (especially GA) and there is not any possibility for unacceptable shapes to be generated during the optimization process.

The values of $\Delta\rho_{max}$, Δz_{max}, and $\Delta\rho_{grd}$ determine the maximum permissible dimensions of antenna. In this work, the chosen values of these parameters are relatively low, which results in relatively small antennas. However, due to the effectiveness of the optimization process and the unique features of volcano smoke antenna, especially the shaped ground, these optimized antennas are possessing proper performances (section 3).

2. 2. Electromagnetic Simulator   An efficient FDTD tool for analyzing the rotationally-symmetric structures (by the name of RSS-FDTD) has been developed to carry out the electromagnetic analysis of antennas. This code is based on the FDTD formulation in cylindrical coordinates taking into account the rotational symmetry of structure and excitation.

Therefore, the performed simulations are two-dimensional instead of three-dimensional and the required memory space and CPU-time are significantly low. The RSS-FDTD code uses a non-uniform mesh generation technique which improves the accuracy of modeling and reduces the memory and CPU-time requirements at the same time. Also during the time-domain simulation, a computational window restricts the computations to parts of space which contain passing waves. This reduces the required CPU-time. With low CPU-time requirements, the implementation of different optimization methods (especially the population-based methods) becomes practicable.

The inputs of the RSS-FDTD code include the specifications of the spectral mask and the structure. The code automatically generates an excitation signal, which fits into the specified spectral mask. For example, Figures 4 and 5 show two modulated Gaussian pulses along with their spectral density which fit into the FCC spectral masks for indoor and handheld systems, respectively.

Figure 2. Replacement of an open polygon with two splines which have same sharpness and different expansion.
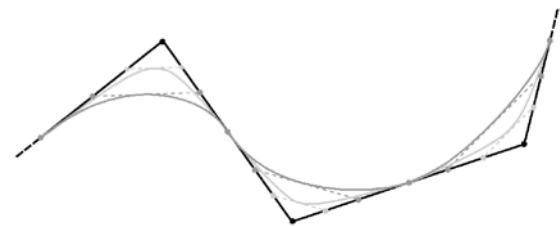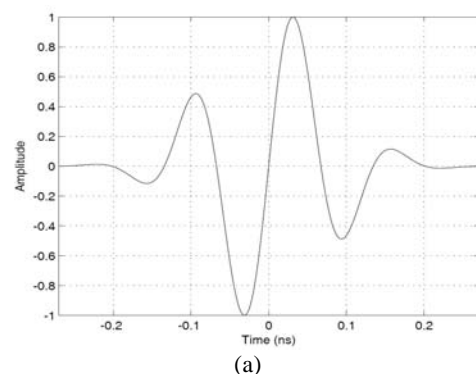

Figure 3. Replacement of an open polygon with two splines which have same expansion and different sharpness.
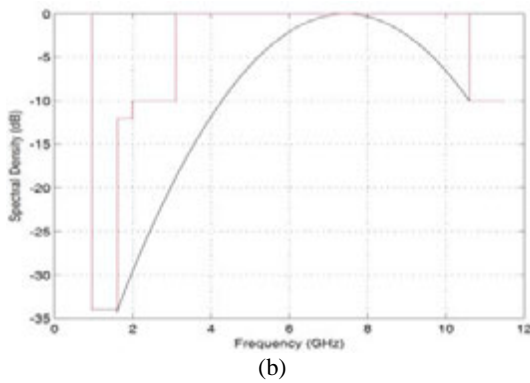

(a)

(b)

Figure 4. (a) A modulated Gaussian pulse and (b) its spectral density which fits into the FCC spectral mask for indoor systems

2. 3. Objective Function   The optimization process has two main goals; minimizing the reflection coefficient of antennas over the operating band and reducing the time-domain distortion of radiated pulses. In some cases, the reduction of variations in the energy pattern is added to these goals. The objective function is a weighted sum of terms, each considered to satisfy one of these goals. The term, which is set to satisfy the first goal, is:

$$F_1 = \max_{f \in [f_b, f_e]} \{R(f)\} \tag{15}$$

where f_b and f_e are the lowest and the highest frequencies in the operating band and $R(f)$ is the reflection coefficient. The term considered for the second goal is:

$$F_2 = \frac{\sum_{n=1}^{n_\theta} W(\theta_n).[1 - CF(\theta_n)]}{\sum_{n=1}^{n_\theta} W(\theta_n)} \tag{16}$$

Here $CF(\theta_n)$ is the normalized correlation between the input signal of antenna ($s_{in}(t)$) and the signal detected by a virtual probe placed at far-zone along a specified direction ($s_{\theta_n}(t)$) and $W(\theta_n)$ is a weight assigned to that direction. n_θ is the number of specified directions. The normalized correlation (correlation factor) is evaluated as follows:

$$CF(\theta) = \max_{\tau} \left\{ \frac{\int s_{in}(t) s_\theta(t - \tau) dt}{\sqrt{\int s_{in}^2(t) dt} \sqrt{\int s_\theta^2(t) dt}} \right\} \tag{17}$$

The weighting for different directions is considered as follows:

$$W(\theta) = \sqrt{1 - \frac{|\theta - 90°|}{90°}} \tag{18}$$

The term, which is considered for the reduction of variations in the energy pattern, is:

$$F_3 = \frac{1}{s(n_\theta - 1)} \sum_{n=1}^{n_\theta} |P(\theta_n)| \tag{19}$$

where

$$P(\theta) = 10 \log \left[\frac{E(\theta)}{\max_n E(\theta_n)} \right] \quad , \quad E(\theta) = \int s_\theta^2(t) dt \tag{20}$$

$P(\theta)$ is the relative average power of pulse in a specified direction which could be expressed in dB. In (19), s is a constant which is set equal to 30.
Finally, the objective function is evaluated as follows:

$$F = c_1 F_1 + c_2 F_2 + c_3 F_3 \tag{21}$$

When optimization is restricted to the main goals, c_1 and c_2 are set equal to 0.65 and 0.35, respectively and the third term is omitted. Otherwise, c_1, c_2, and c_3 are set equal to 0.4, 0.2, and 0.4, respectively.

TABLE 1. Settings for Different Options of GA Optimizer

Options	Settings
Population size	120
Fitness Scaling	Rank
Selection	Stochastic Uniform
Elite Count	2
Crossover	Scattered
Crossover Fraction	0.8
Mutation	Adaptive Feasible
Generations	10
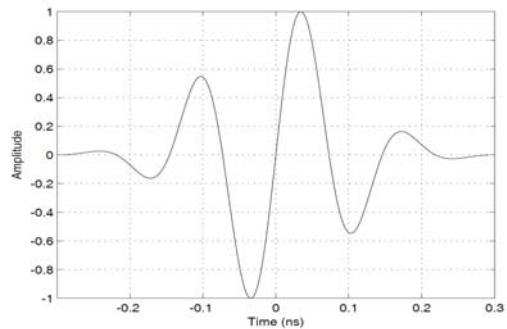
(a)
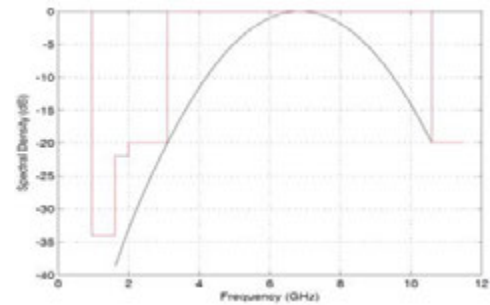
(b)

Figure 5. (a) A modulated Gaussian pulse and (b) its spectral density which fits into the FCC spectral mask for handheld systems.

2. 4. Optimization Procedure   The variety of possible geometries and the high number of optimization parameters raise the possibility of having different optimum designs. In other words, the objective function may have multiple local minimums in the search domain. Consequently, global optimization methods should be used in order to search for the best design. Moreover, the process of calculating the objective function for each antenna structure is relatively complex and lengthy, including the electromagnetic simulation of antenna and the computation of characteristics which are involved in the definition of objective function. Therefore, the implementation of heuristic strategies is necessary in order to reduce the overall time needed for the completion of the optimization process. On the other hand, the final stages of optimization with heuristic strategies are subjected to stagnation.Hence, it is better to complete the global optimization by implementing a local optimization method.

In this work, the optimization of UWB antennas is performed by applying a hybrid procedure. First, the global optimization is carried out using the Matlab GA optimizer. Then, the procedure is completed by a local optimization using the pattern search method.

3. NUMERICAL RESULTS

In this section, three optimized profiles for UWB antenna with finite ground plane are presented which are obtained by the predescribed optimization process. In all three cases, the optimization process is performed to design antennas suitable for UWB indoor applications. Antennas are fed through a 50 Ω coaxial line. The values of both $\Delta\rho_{mar}$ and Δz_{mar} are chosen equal to 2.5 cm. The options of the GA optimizer are set as shown in Table 1. These settings are found by trial and error.

During the GA search, all expansion and sharpness factors are fixed at 1 and 0.5, respectively. However, during the pattern search, these factors are considered as tunable parameters. To calculate the value of objective function, f_b and f_e in (15) are set equal to 3.1 GHz and 10.6 GHz, respectively. Also, the values of θ_n in (16) and (19) are chosen equal to 90˚, 60˚, and 30˚.

The first antenna profile is obtained considering a flat ground ($z_{U_i} = 0$, i = 0, 1, 2) and $\Delta\rho_{max}$, $\Delta\rho_{grd}$, and Δz_{max} equal to 3 cm, 1.5 cm, and 4 cm, respectively. Moreover, optimization is restricted to the main goals. This antenna is used as a prototype to show the effects of shaped ground on the second and third antennas. Figure 6 shows the first antenna profile. The diameter and height of antenna and the diameter of ground plane are 5.47 cm, 3.82 cm, and 8.77 cm, respectively. In this case, the optimization process has resulted in a hollow conical shape for radiating element. This shape provides a gradual transition of radiating pulse from feed line to free space. In addition, with this shape, the current distribution on radiating element could be extended into conical hole. Therefore, the radiating element could have higher electrical length in spite of restrictions on antenna size. It should be noted that a hollow radiating element is more difficult to manufacture.
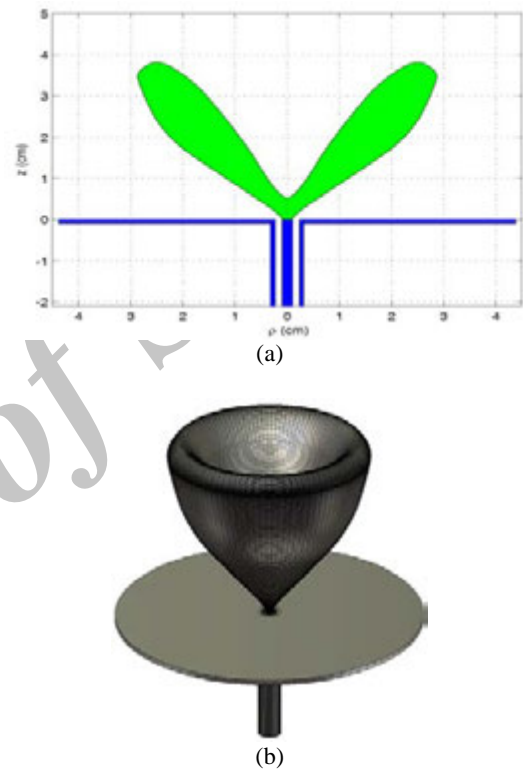

(a)

(b)

Figure 6. (a) The first optimized profile for UWB monopole antenna with finite ground plane and (b) the 3-D view of antenna
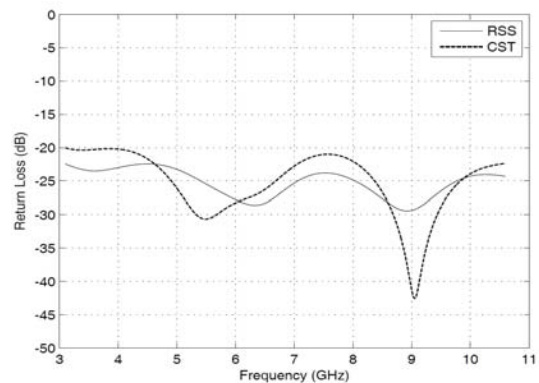

Figure 7. Return loss of the first optimized antenna calculated by RSS-FDTD (solid line) and CST Microwave Studio (dashed line).

Figure 7 presents the return loss of antenna in 3.1-10.6 GHz band calculated by RSS-FDTD and CST Microwave Studio software which is based on finite integration technique (FIT). It must be noted that the CST software is not used in the optimization process. The CST calculated data are only prepared for the resulted optimized antenna. The maximum return loss in this band is -22.4 dB. Figure 8 shows the correlation factor at different elevation angles. The correlation factor is above 0.95 between $33°$ and $122°$. Figure 9 presents the energy pattern of the antenna. The average power of pulse at $\theta = 90°$ is 4 dB less than maximum. According to the geometrical theory of diffraction, radiated wave at each point in the shadow region of ground plane is the sum of two diffracted waves coming from the nearest and the farthest points on ground edge. At point near the axis of symmetry ($\theta = 180°$), these two waves arrive with little time difference. Nevertheless, away from this axis, these waves arrive with more time difference, resulting in more distortion of waveform and less correlation factor. This explains the minimum in correlation factor curve at $\theta = 150°$. The minimum in energy pattern at $\theta = 147.5°$ could be explained in a similar manner. The second antenna profile is obtained considering a shaped ground (with u_{12}=0.15) and the same values for $\Delta \rho_{max}$, $\Delta \rho_{grd}$, and Δz_{max} as in the previous case. In this case, the reduction of variations in the energy pattern is added to the optimization goals. Figure 10 shows the second antenna profile. The diameter and height of the antenna and the diameter of ground plane are 5.70 cm, 3.71 cm, and 6.41 cm, respectively. Figure 11 presents the return loss of antenna. The maximum return loss in 3.1-10.6 GHz band is -27.8 dB. The radiated waveforms at $\theta = 90°$, $\theta = 60°$, and $\theta = 30°$ (calculated by RSS-FDTD and CST Microwave Studio) and their spectral density are shown in Figures 12, 13, and 14, respectively. Figure 15 shows the correlation factor at different elevation angles. Figure 16 presents the energy pattern of the antenna. The average power of pulse at $\theta = 90°$ is 1.6 dB less than maximum which shows 2.4 dB improvement compared to the first antenna.
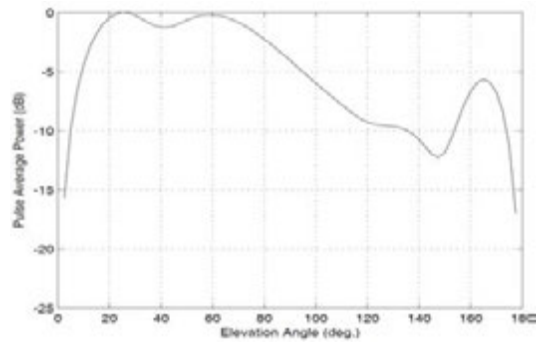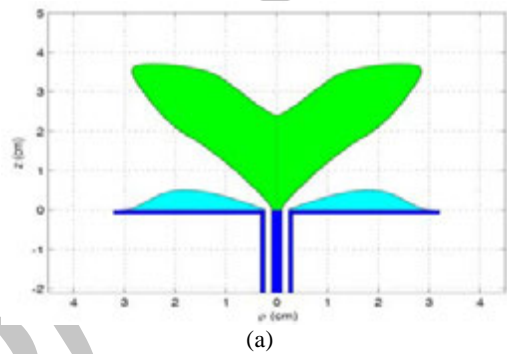

Figure 9. Energy pattern of the first optimized antenna

(a)

(b)

Figure 10. (a) The second optimized profile for UWB monopole antenna with finite ground plane and (b) the 3-D view of antenna
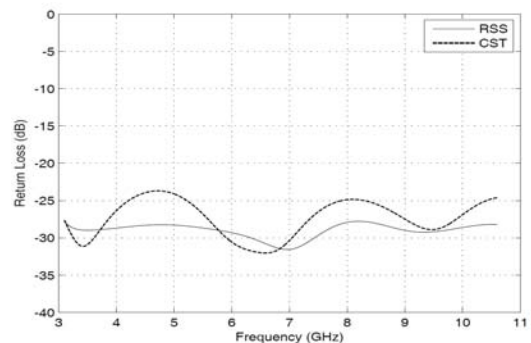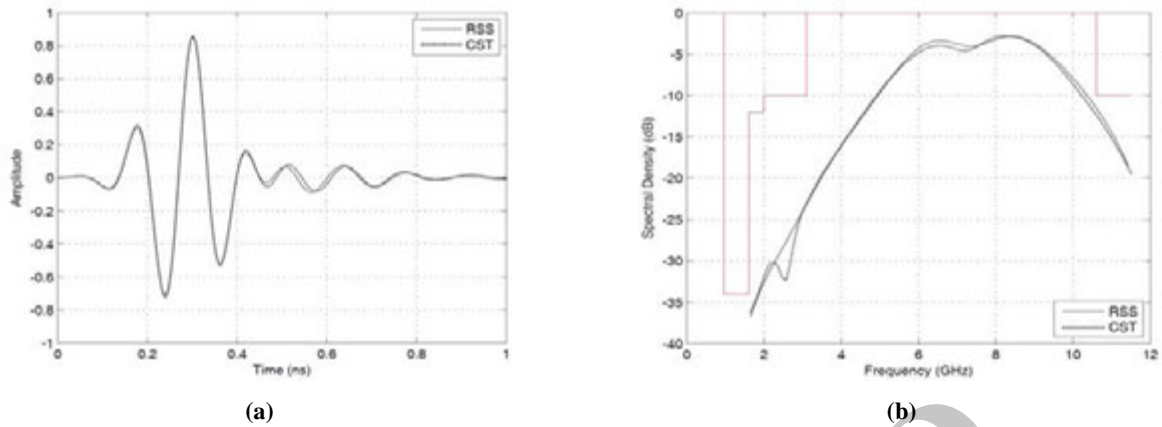

Figure 8. Correlation factor for the first optimized antenna as a function of elevation angle.

Figure 11. Return loss of the second optimized antenna calculated by RSS-FDTD (solid line) and CST Microwave Studio (dashed line)

(a)   **(b)**

Figure 12. (a) Radiated waveform of the second optimized antenna at $\theta = 90°$ and (b) its spectral density

(a)   **(b)**
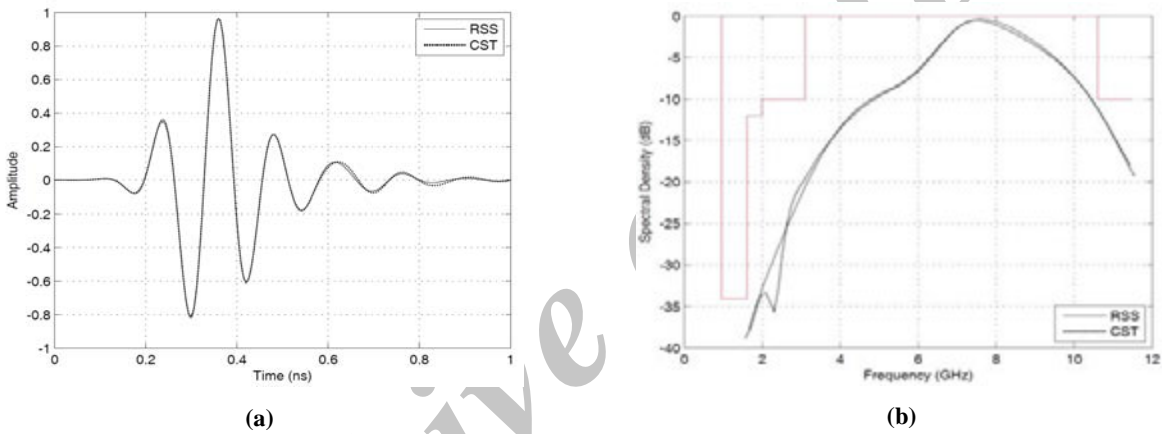
Figure 13. (a) Radiated waveform of the second optimized antenna at $\theta = 60°$ and (b) its spectral density
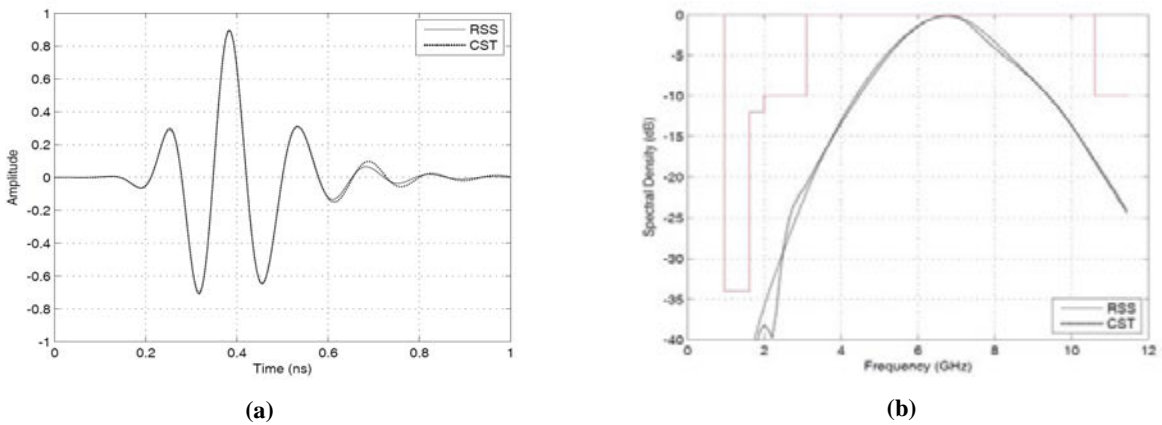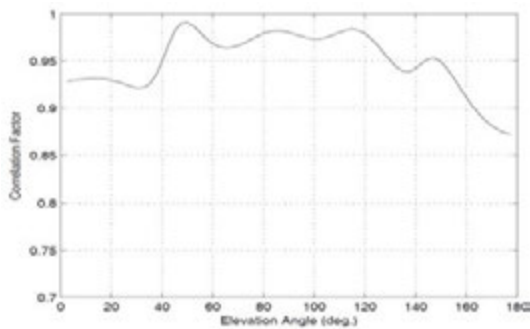

(a)   **(b)**

Figure 14. (a) Radiated waveform of the second optimized antenna at $\theta = 30°$ and (b) its spectral density.

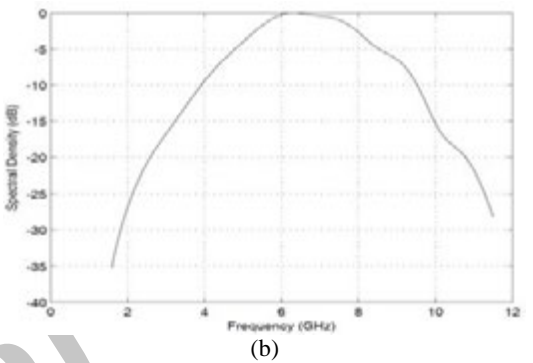Figure 17 shows a pair of second optimized antennas placed 60 cm away from each other in free space which are operating as transmitter and receiver. Figure 18 presents the signal at output terminals of the receiving antenna calculated by means of CST Microwave Studio

software. The spectral density of signal is also shown in this figure. The normalized correlation between the input signal of transmitting antenna and the output signal of receiving antenna is 0.89. The magnitude and phase of transfer function (S_{21}) are shown in Figure 19.

The corresponding group delay (τ_g) is shown in Figure 20. The widest variations of $|S_{21}|$ and τ_g in 3.1-10.6 GHz band are less than 12.3 dB and 0.15 ns, respectively. It could be observed that by shaping the ground, the optimized antenna acquires smaller size and better performance. Especially, the diameter of ground plane reduces, because the shaped ground has higher electrical length. In addition, the radiating element has a smaller hole which makes the manufacturing much easier. The third antenna profile is obtained letting the shaped ground to rise higher (with $u_{12} = 0.4$) resulting in a volcano smoke antenna. The values of $\Delta\rho_{max}$, $\Delta\rho_{grd}$, and Δz_{max} are set to 1.5 cm, 0. 5 cm, and 3.5 cm, respectively. Figure 21 shows the profile of the third antenna. Antenna has a diameter and height of 3.38 cm and 3.23 cm, respectively. The diameter of ground plane is 4.06 cm. The return loss of antenna is shown in Figure 22. The maximum return loss in 3.1-10.6 GHz band is -27.8 dB.

(a)

(b)

Figure 18. (a) Signal at the output terminals of the receiving antenna (Figure 17) and (b) its spectral density

Figure 15. Correlation factor for the second optimized antenna as a function of elevation angle

Figure 16. Energy pattern of the second optimized antenna

Figure 17. A pair of second optimized antenna placed 60 cm away from each other in free space which are operating as transmitter and receiver
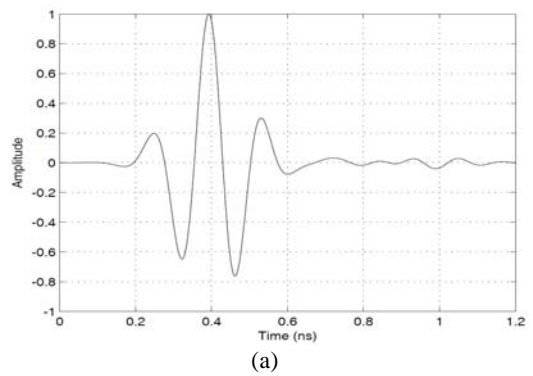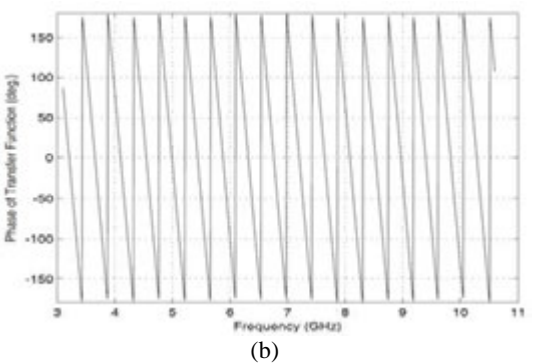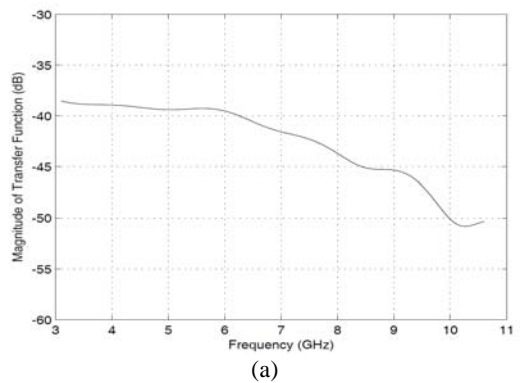

(a)

(b)

Figure 19. Transfer Function of the two-antenna system shown in Figure 17. (a) Magnitude and (b) phase
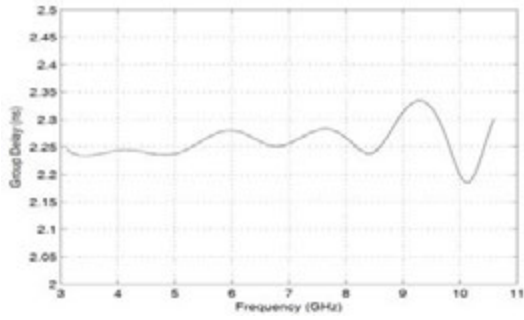
Figure 20. Group delay in two-antenna system shown in Figure 17

(b)

Figure 21. (a) The third optimized profile for UWB monopole antenna with finite ground plane (the volcano smoke antenna) and (b) the 3-D view of antenna
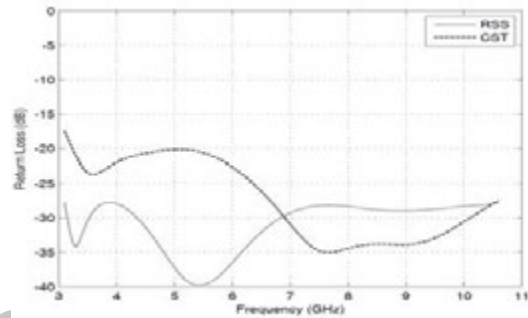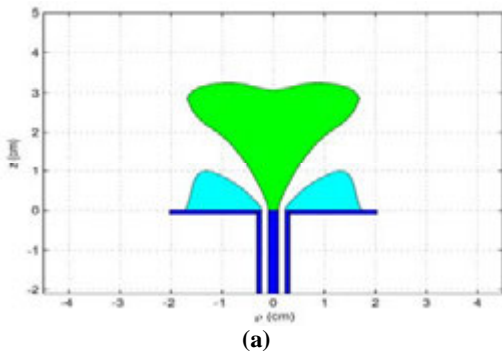

(a)

Figure 22. Return loss of the third optimized antenna calculated by RSS-FDTD (solid line) and CST Microwave Studio (dashed line)
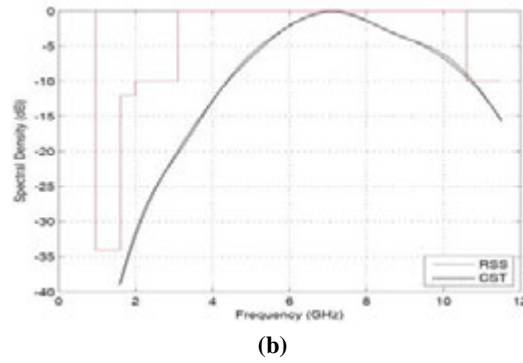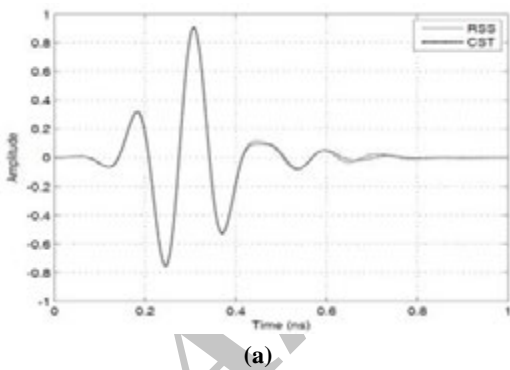

(a)

(b)

Figure 23. (a) Radiated waveform of the third optimized antenna at $\theta = 90°$ and (b) its spectral density

(a)

(b)
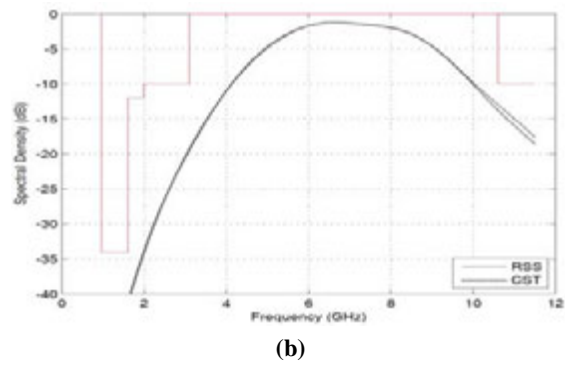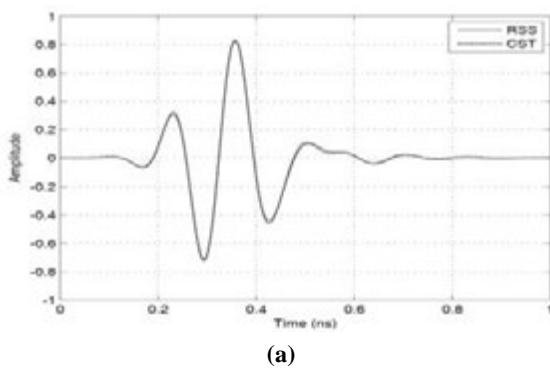
Figure 24. (a) Radiated waveform of the third optimized antenna at $\theta = 60°$ and (b) its spectral density.

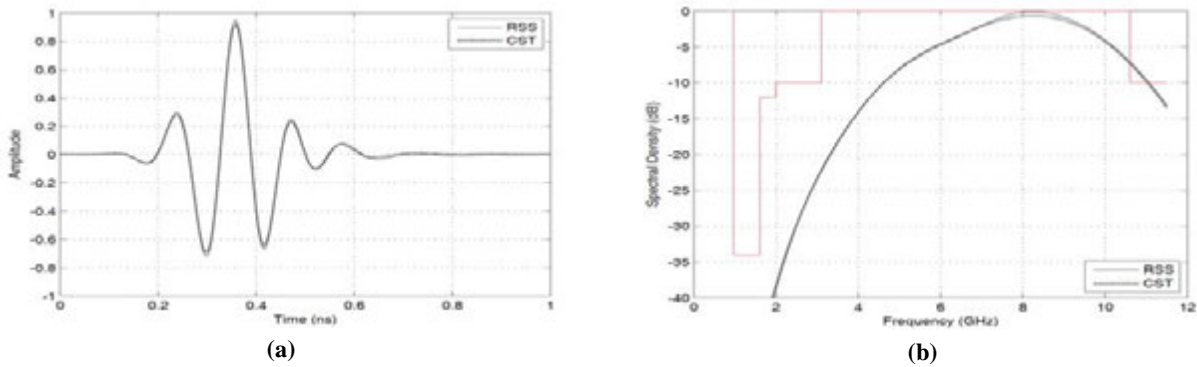**(a)**   **(b)**

Figure 25. (a) Radiated waveform of the third optimized antenna at $\theta = 30°$ and (b) its spectral density
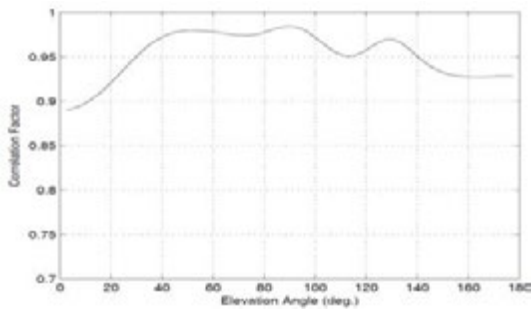

Figure 26. Correlation factor for the third optimized antenna as a function of elevation angle
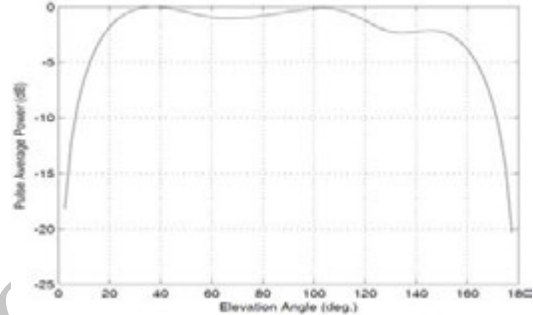

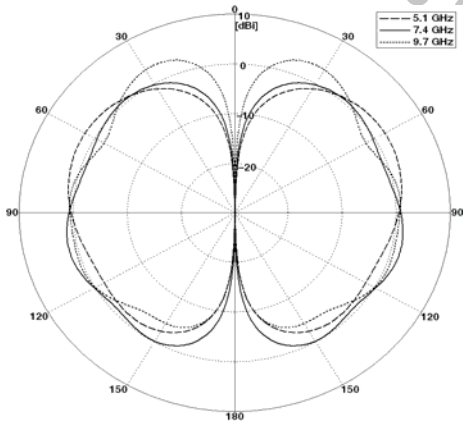**Figure 27.** Energy pattern of the third optimized antenna

Figure 28. Radiation (directivity) pattern of the third optimized antenna at 5.1 GHz, 7.4 GHz, and 9.7 GHz.

The radiated waveforms at $\theta = 90°$, $\theta = 60°$, and $\theta = 30°$ and their spectral density are shown in Figure 23, Figure 24, and Figure 25, respectively. Figure 26 presents the correlation factor at different elevation angles. The correlation factor is above 0.95 between 30° and 140°, which shows considerable improvement compared to the first and second antennas.

The energy pattern of the antenna is shown in Figure 27. This antenna has a smooth energy pattern in E-plane and the average power of pulse at $\theta = 90°$ is only 0.4 dB less than maximum.

Also, Figure 28 shows the radiation (directivity) pattern of the antenna at 5.1 GHz, 7.4 GHz, and 9.7 GHz. The spectral density of the excitation signal has its maximum value at 7.4 GHz (Figure 4) and it reduces by 6 dB at 5.1GHz and 9.7 GHz. Figure 28 illustrates that for the third optimized antenna, the general form of radiation pattern does not change drastically with frequency.

Three transmitting-receiving systems are considered for this antenna. The first system is similar to the one shown in Figure 17 consisting of two parallel antennas placed 60 cm away from each other. But, in the second and third systems, the transmitting antenna is rotated $45°$ towards or opposite to the receiving antenna.

Figure 29 presents signals at output terminals of the receiving antenna and their spectral densities. The normalized correlation between the input and output signals in first, second, and third transmitting-receiving systems is 0.84, 0.85, and 0.86, respectively. Although the energy of output signal is reducing by turning the transmitting antenna, the similarity between the input and output signals does not change so much.
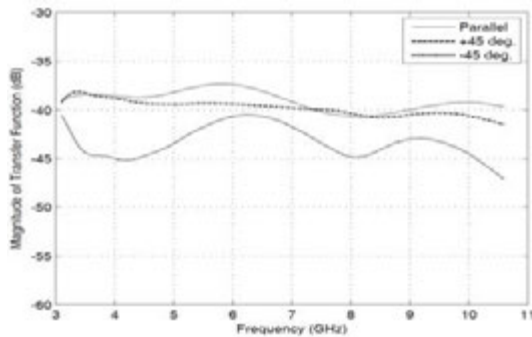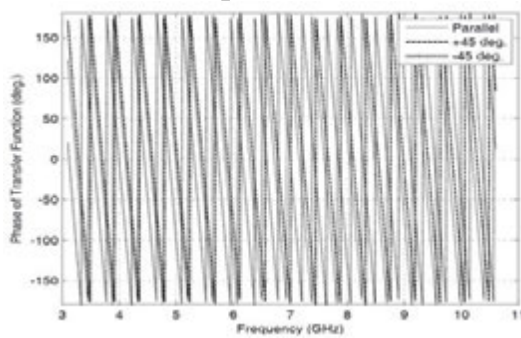
Figure 31. Group delay in two-antenna systems (calculated for the third optimized antenna)
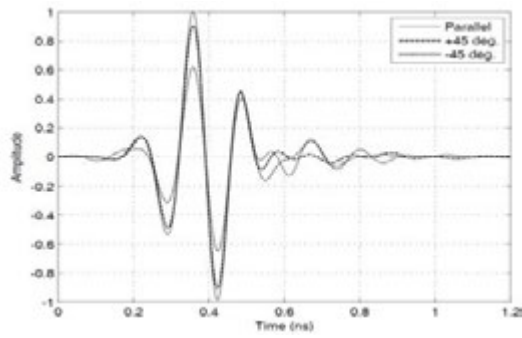
(a)
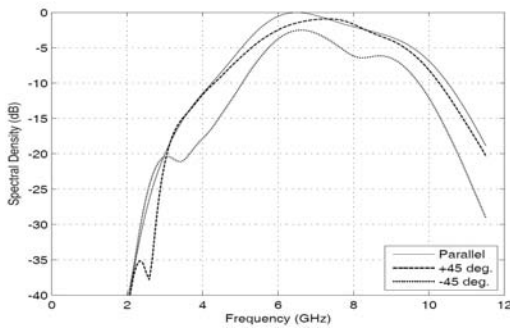
(b)

Figure 29. (a) Signals at the output terminals of the receiving antenna and (b) their spectral densities (calculated for the third optimized antenna)

(a)

(b)

Figure 30. Transfer Functions of two-antenna systems. (a) Magnitude and (b) phase (calculated for the third optimized antenna)
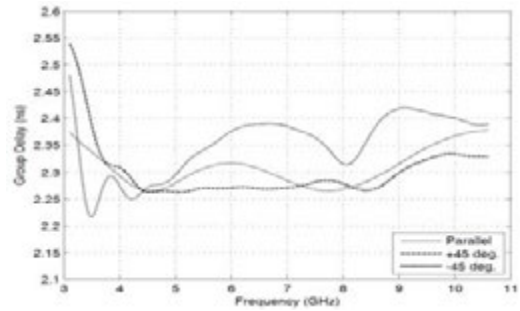
The magnitude and phase of transfer functions are shown in Figure 30. In addition, Figure 31 shows the corresponding group delay. The widest variations of $|S_{21}|$ and τ_g in 3.1-10.6 GHz band for the first two-antenna system are only 3.3 dB and 0.11 ns, respectively, which shows 9 dB and 0.04 ns improvement compared to the second antenna. Variation of $|S_{21}|$ is almost the same for the second system (3.4 dB) and it is increased for the third one (6.5 dB). Variation of τ_g is increased for both second and third systems (0.28 ns and 0.26 ns, respectively). It could be observed that in a transmitting-receiving system formed by a pair of third optimized antennas, the inclination of one antenna (relative to the other) does not severely degrade the performance.

These results show that by letting the shaped ground to rise higher, even with tighter restrictions on dimensions of antenna, further improvements in characteristics is achievable. This is partly because the shaped ground in this case provides a more gradual transition of radiating pulse.

4. CONCLUSION

In this paper, the design of a novel volcano smoke antenna for UWB indoor applications has been presented. The design method is based on a general description for the geometry of UWB monopole antennas, which is capable of producing most possible shapes for these antennas. It is also compatible with different optimization methods. In addition to a volcano smoke antenna, this method has been used to design two optimized monopole antennas with flat and shaped grounds. The optimization of antennas has been carried out by applying a hybrid procedure, which begins with a GA global search and completes with a local search. The optimization process aims at minimizing the reflection coefficient of antennas over the operating band while reducing the time-domain distortion of radiated pulses. For Shaped ground and volcano smoke

antennas, the reduction of variations in the energy pattern has been added to the optimization goals. The numerical results show the reliability and effectiveness of the whole process. These results also show considerable improvement regarding the size and operational characteristics of antenna in comparison with similar antennas reported in the literature [13], [17].

The operational characteristics of shaped ground and volcano smoke antennas show that by shaping the ground, better performance could be achieved with smaller radiating elements and ground planes, because shaped ground provides a gradual transition of radiating pulse from feed line to free space. In addition, the shaped ground has higher electrical length.

5. REFERENCES

1. Kraus, J. D., "Antennas", 2nd edition, New York, McGraw-Hill, (1988).

2. Commission, F. C., "Revision of part 15 of the commission's rules regarding ultra-wideband transmission systems", *First Report and Order, FCC*, Vol. 2, No., (2002), V48.

3. Allen, O. E., Hill, D. A. and Ondrejka, A. R., "Time-domain antenna characterizations", *Electromagnetic Compatibility, IEEE Transactions on*, Vol. 35, No. 3, (1993), 339-346.

4. Lamensdorf, D., and Susman, L., "Broadband-pulse antenna techniques", *IEEE Antennas and. Propagation Magazine*, Vol. 36, No. 1, (1994), 20-30.

5. McLean, J. S., Foltz, H. and Sutton, R., "Pattern descriptors for UWB antennas", *Antennas and Propagation, IEEE Transactions on*, Vol. 53, No. 1, (2005), 553-559.

6. Taniguchi, T. and Kobayashi, T., "An omnidirectional and low-VSWR antenna for ultra-wideband wireless systems", in Radio and Wireless Conference, IEEE, (2002), 145-148.

7. Paulsen, L., West, J., Perger, W. and Kraus, J., "Recent investigations on the volcano smoke antenna", in Antennas and Propagation Society International Symposium, IEEE, Vol. 3, (2003), 845-848.

8. Simpson, T., "Influence of profile shape on the bandwidth of a rotationally symmetric monopole", in Antennas and Propagation Society International Symposium (APSURSI), IEEE, (2010), 1-4.

9. Telzhensky, N. and Leviatan, Y., "Novel method of UWB antenna optimization for specified input signal forms by means of genetic algorithm", *Antennas and Propagation, IEEE Transactions on*, Vol. 54, No. 8, (2006), 2216-2225.

10. Telzhensky, N. and Leviatan, Y., "Planar differential elliptical UWB antenna optimization", *Antennas and Propagation, IEEE Transactions on*, Vol. 54, No. 11, (2006), 3400-3406.

11. Kim, J., Yoon, T. and Choi, J., "Design of an ultra wide-band printed monopole antenna using FDTD and genetic algorithm", *Microwave and Wireless Components Letters, IEEE*, Vol. 15, No. 6, (2005), 395-397.

12. Kajenski, P. J., "Particle swarm optimization of antenna elements for foliage penetrating radar", in Radar Conference, IEEE, (2007), 449-450.

13. Martinez-Fernandez, J., Gil, J. M. and Zapata, J., "Ultrawideband optimized profile monopole antenna by means of simulated annealing algorithm and the finite element method", *Antennas and Propagation, IEEE Transactions on*, Vol. 55, No. 6, (2007), 1826-1832.

14. Lizzi, L., Viani, F., Azaro, R. and Massa, A., "Optimization of a spline-shaped UWB antenna by PSO", *Antennas and Wireless Propagation Letters, IEEE*, Vol. 6, (2007), 182-185.

15. Cerny, P. and Mazanek, M., "Simulated transient radiation characteristics of optimized ultra wideband printed dipole antennas", in Radioelektronika, 17th International Conference, IEEE, (2007), 1-6.

16. Lizzi, L., Viani, F., Azaro, R. and Massa, A., "A PSO-driven spline-based shaping approach for ultrawideband (UWB) antenna synthesis", *Antennas and Propagation, IEEE Transactions on*, Vol. 56, No. 8, (2008), 2613-2621.

17. Martinez-Fernandez, J., Gil, J. and Zapata, J., "Profile optimisation in planar ultra-wideband monopole antennas for minimum return losses", *Microwaves, Antennas & Propagation, IET*, Vol. 4, No. 7, (2010), 881-892c.

18. Dumoulin, A., John, M., Ammann, M. J. and McEvoy, P., "Optimized monopole and dipole antennas for UWB asset tag location systems", *Antennas and Propagation, IEEE Transactions on*, Vol. 60, No. 6, (2012), 2896-2904.

19. Paran, K., Fardis, M. and Abolghasemi, A., "Searching for the Optimal Shapes of Ultra-Wideband Monopole Antennas", in International Symposium on Antennas and Propagation (ISAP),: Taipei, Taiwan, (2008), 401-404.

20. Rahmat-Samii, Y. and Michielssen, E., "Electromagnetic optimization by genetic algorithms", John Wiley and Sons, (1999).

21. MathWorks, T., "Genetic algorithm and direct search toolbox user's guide", (2005).

A Novel Volcano Smoke Antenna with Optimal Shape

K. Paran[a], A. Abolghasemi [b]

a Department of Electrical and Computer Engineering, S. Beheshti University, Tehran, Iran
b Department of Communications Technology, Research Institute for information and Communications Technology, Tehran, Iran

چکیده

در این مقاله چگونگی طراحی آنتنی جدید از نوع «دودآتشفشان» ارائه شده است. روش طراحی بر پایه توصیفی فراگیر برای شکل هندسی آنتن‌های تک‌قطبی فراپهن‌باند است که توانایی ایجاد بیشتر شکل‌های ممکن برای این آنتن‌ها را دارا می‌باشد. این روش همچنین با شیوه‌های بهینه‌سازی گوناگون سازگار است. افزون بر آنتن دودآتشفشان، این روش برای طراحی دو آنتن تک‌قطبی بهینه‌سازی‌شده با صفحه‌های زمین «تخت» و «شکل‌داده‌شده» به کار رفته است. جستجو برای آنتن‌های بهینه، با استفاده از «الگوریتم ژنتیک» به انجام می‌رسد و با به‌کارگیری یک روش محلی تکمیل می‌گردد. روند بهینه‌سازی به هدف کاهش بازتاب از آنتن‌ها در باند کاری و کاهش واپیچش پالس‌های تابشی در حوزه زمان به انجام می‌رسد. برای آنتن با زمین شکل‌داده‌شده و آنتن دودآتشفشان کاهش نوسان‌ها در الگوی تابشی انرژی نیز به هدف‌ها افزوده می‌شود. نتایج عددی، دقت و کارامدی کل روند را نشان می‌دهند. نتایج همچنین نشان‌دهنده‌ی بهبود قابل توجهی از نظر اندازه و مشخصات کارکردی آنتن‌ها نسبت به موارد همانندِ گزارش‌شده است. مشخصات کارکردی آنتن با زمین شکل‌داده‌شده و آنتن دودآتشفشان مشخص می‌سازد که با شکل‌دهی زمین می‌توان به آنتن‌هایی کوچک‌تر با کارایی بهتر دست یافت.

doi: *10.5829/idosi.ije.2013.26.03c.06*